Mathematics Interdisciplinary Research **6** (2021) 35 − 61

*Original Scientific Paper*

# Schwinger Pair Creation by a Time-Dependent Electric Field in de Sitter Space with the Energy Density $E_\mu E^\mu = E^2 a^2(\tau)$

*Fatemeh Monemi and Farhad Zamani* ⋆

**Abstract**

We investigate Schwinger pair creation of charged scalar particles from a time-dependent electric field background in (1+3)-dimensional de Sitter spacetime. Since the field's equation of motion has no exact analytical solution, we employ *Olver's uniform asymptotic approximation method* to find its analytical approximate solutions. Depending on the value of the electric field $E$, and the particle's mass $m$, and wave vector $\mathbf{k}$, the equation of motion has two turning points, whose different natures (real, complex, or double) lead to different pair production probability. More precisely, we find that for the turning points to be real and single, $m$ and $\mathbf{k}$ should be small, and the more smaller are the easier to create the particles. On the other hand, when $m$ or $\mathbf{k}$ is large enough, both turning points are complex, and the pair creation is exponentially suppressed. In addition, we study the pair creation in the weak electric field limit, and find that the semi-classical electric current responds as $E^{1-2\sqrt{\mu^2}}(1-\ln E)$, where $\mu^2 = \frac{9}{4} - \frac{m_{\rm ds}^2}{H^2}$. Thus, below a critical mass $m_{\rm cr} = \sqrt{2}H$, the current exhibits the infrared hyperconductivity.

Keywords: Schwinger mechanism, electromagnetic processes, time-dependent electric field, uniform asymptotic approximation.

2010 Mathematics Subject Classification: 81T20, 81V10, 34E20.

**How to cite this article**

F. Monemi and F. Zamani, Schwinger pair creation by a time-dependent electric field in de Sitter space with the energy density $E_\mu E^\mu = E^2 a^2(\tau)$, *Math. Interdisc. Res.* **6** (2021) 35 − 61.

⋆Corresponding author (E-mail: zamani@kashanu.ac.ir)

Academic Editor: Majid Moemzadeh

Received 9 October 2019, Accepted 2 February 2020

DOI: 10.22052/mir.2020.204420.1167

# 1. Introduction

A strong enough external electric field can produce pairs of charged particles from vacuum. This non-perturbative phenomenon in quantum field theory, that was originally proposed by Sauter [31] and further investigated by Heisenberg and Euler [18], is known as the Schwinger effect after the work of Schwinger [32] in which a complete theoretical description is given (see, e.g., [10] for a recent review). With a uniform background electric field $E$ in flat spacetime, the number density (probability) of the created pairs is proportional to the factor $\exp\left(-\pi m^2/eE\right)$, where $m$ and $e$ are the particle mass and charge (coupling), respectively. This pocket formula shows that the pair production occurs when the electric field is as strong enough as a critical field $E_{\rm cr} \simeq m^2/e$; otherwise it is exponentially suppressed. For the lightest charged particle, the electron, we need an intense field $E_{\rm cr} \simeq 1.3 \times 10^{18}$ V/m [6] that is still experimentally far-reaching. This is the main obstacle to directly observe the Schwinger pair production in ground-based experiments. Nevertheless, as pointed out in the review article [30], one could search for the imprint of the Schwinger effect in astrophysical and cosmological contexts where extremely intense background fields could naturally be present. This could be done, e.g., by considering the backreaction of the created pairs or the signature of the induced current on the magnetogenesis and inflation.

De Sitter (dS) geometry plays a crucial role in our current understanding of cosmology. Specifically, the inflationary background in the early universe (see, e.g., [2, 22] for reviews) as well as the present day accelerated expansion of the universe (see, e.g., [5] for review) is approximately described by dS spacetime. Widely motivated from false vacuum decay and bubble nucleation to cosmological applications including magnetogenesis or giving a thermal interpretation, Schwinger mechanism in dS background has been extensively studied for various types of particles and spacetime dimensions [3, 4, 8, 9, 16, 17, 19, 21, 34, 36, 37]. Thanks to the curvature of the spacetime, Schwinger pair creation mechanism in $1+1$-dimensional dS geometry showed some quite peculiar features [8, 9, 19, 36, 37]. In particular, in the case of light fields, the current induced by created particles is inversely proportional to the applied electric field which leads to the so-called infrared hyperconductivity. The analysis, extended to $1+3$-dimensional dS spacetime, showed further unexpected results [16, 17, 21]. Furthermore, in [3], it is shown that the Schwinger effect tends to have the similar aspects even in $1+d$-dimensional dS background. However, it is claimed recently that the unintuitive infrared behavior (negative conductivity) of the induced Schwinger current in dS space might be an artifact of regularization schemes [1].

Most of the previous works assumed a uniform background electric field with constant energy density to consider Schwinger effect in dS space, which is in contrast with the realistic situation. Indeed, the background electric field would be changed due to the backreaction of the created pairs and the expansion of the universe. More importantly, the constancy of the energy density violates the second law of thermodynamics in the case of a homogeneous field configuration in an

expanding conformally flat background [12]. Recently, in some realistic models, Schwinger pair production by time-dependent inflation-driven electric field and its backreaction to the background geometry has been investigated [11, 20, 33]. These studies employ the fact that during the anisotropic inflation a persistent electric field can be established by introducing a time-dependent gauge kinetic coupling between the inflation and the gauge field [7, 39]. It is shown that, for light charged scalar field, the pair production probability is strongly enhanced in the weak electric field limit and the infrared hyperconductivity also occurs in anisotropic inflation [11]. On the other hand, in the strong-field regime, it is shown that the Schwinger current has the same functional dependence as in the case of a constant electric field [20].

Unlike the case of flat space, studying the Schwinger effect in time-dependent electric field background has been limited to some special cases in curved spacetime (see, e.g., [14, 15, 23, 35, 38]). This is mainly because, in the presence of a time-dependent background in curved spacetime, it is generally difficult to solve the field's equations of motion to find the mode functions and interpret them in terms of positive- and negative-frequency modes. Thus, one needs either to choose a special form for the scale factor or to restrict himself/herself to a particular time-dependent electric field. Nevertheless, one can resort to approximate methods. Based on Olver's *uniform asymptotic approximation method* for the solution of the second-order differential equation with two turning points [26], the Schwinger effect coupled to inflation has been recently studied in [11] with the focus on the weak electric field and light mass limits. In the present work, we use this uniform asymptotic theory, that was developed further in [41, 42, 43, 44], to investigate the Schwinger pair creation by a time-dependent electric field in de Sitter spacetime. For different parameter region (different cases of the turning points), we compute the pair production probability and study its different features. We show that the pair creation is enhanced for light scalar fields, while is suppressed exponentially for massive particles. We also compute the semi-classical electric current in the weak electric field limit and show that the negative conductivity occurs.

The rest of the article is organized as follows. In Section 2, we first introduce the setup (i.e., the background spacetime and the time-dependent electric fields). Then, starting from the action, we obtain the equation of motion for a charged scalar field in these backgrounds. We show that the problem of finding the mode functions is reduced to solve a second-order differential equation which does not admit an exact analytical solution. We briefly introduce the uniform asymptotic approximation method in Section 3 and use it to find the approximate mode functions. We use these approximate mode functions to define the "*in*" and "*out*" vacuum states for the quantized scalar field, and compute the Bogoliubov coefficients and pair production probability in Section 4. Then, we explore the different features of the pair creation for the different parameter regions (that lead to different natures for the turning points). Finally, we conclude in Section 5. The appendix include some useful information on Weber's equation, parabolic cylinder functions and their asymptotic expansion.

## 2. The Field's Equation of Motion

We take the background spacetime to be the four-dimensional de Sitter ($dS_4$) space, that is described by the metric

$$ds^2 = g_{\mu\nu}\, dx^\mu dx^\nu = a^2(\tau)(-d\tau^2 + d\mathbf{x}^2), \qquad \mathbf{x} = (x, y, z) \in \mathbb{R}^3, \tag{1}$$

where $a(\tau)$ is the scale factor, and the conformal time $\tau$ is related to the physical time $t$ by $dt = a d\tau$. Note that we work in the flat slicing (Poincaré patch) of $dS_4$ space that covers only half of the $dS_4$ manifold. In terms of the Hubble constant $H := a^{-1}(t)\frac{da(t)}{dt} = a^{-2}(\tau)\frac{da(\tau)}{d\tau}$, the conformal time $\tau$ is given by

$$\tau = -\frac{1}{Ha(\tau)}, \qquad \tau \in (-\infty, 0).$$

In this background spacetime, we consider a complex scalar field $\varphi(x)$ with charge $e$ and mass $m$ coupled to a $U(1)$ gauge field $A^\mu(x)$ with the action

$$\mathcal{A} = \int d^4x \sqrt{-g} \left\{ -g^{\mu\nu}(\mathcal{D}_\mu\varphi)^*(\mathcal{D}_\nu\varphi) - (m^2 + \xi R)\varphi^*\varphi - \frac{1}{4}F_{\mu\nu}F^{\mu\nu} \right\}, \tag{2}$$

where $g$ is the determinant of the metric tensor, $\xi$ is the dimensionless nonminimal coupling constant, $R = 12H^2$ is the Ricci scalar curvature, $\mathcal{D}_\mu := \nabla_\mu + ieA_\mu$, and $F_{\mu\nu} = \nabla_\mu A_\nu - \nabla_\nu A_\mu = \partial_\mu A_\nu - \partial_\nu A_\mu$.

We also treat the $U(1)$ gauge field $A_\mu(x)$ as a background field giving rise to a homogenous time-dependent electric field in the $z$-direction. We choose the homogenous vector potential to be

$$A_\mu(\tau) = -\frac{E}{2H^3\tau^2}\,\delta^z_\mu = -\frac{E}{2H}\,a^2\,\delta^z_\mu, \tag{3}$$

such that a co-moving observer with four-velocity $u^\mu$ ($\mathbf{u} = 0$, $u_\mu u^\mu = -1$) measures the electric field $E_\mu = u^\nu F_{\mu\nu} = Ea^2(\tau)\,\delta^z_\mu$ with a growing (time-dependent) energy density $E_\mu E^\mu = E^2a^2(\tau)$. Here $E$ is a positive constant having the dimension $(\text{length})^{-2}$ in natural units. The de Sitter scale $H^{-1}$ has the length dimension and therefore $A_\mu$ has the dimension $(\text{length})^{-1}$.

The equation of motion for the scalar field $\varphi$ can be easily deduced from the action (2) as

$$\Big[\nabla_\mu\nabla^\mu + 2\,ieg^{\mu\nu}A_\mu\nabla_\nu - e^2g^{\mu\nu}A_\mu A_\nu - m^2_{\rm ds}\Big]\varphi(x) = 0,$$

where $\nabla_\mu\nabla^\mu = \frac{1}{\sqrt{-g}}\,\partial_\mu(\sqrt{-g}g^{\mu\nu}\partial_\nu)$ and we defined $m^2_{\rm ds} := m^2 + \xi R$. In the presence of the time-dependent gauge field (3) in the background metric (1), the equation of motion for $\varphi$ takes the explicit form

$$\varphi'' + 2\frac{a'}{a}\varphi' - \partial_i^2\varphi + i\frac{eE}{H}\,a^2\partial_z\varphi + \frac{e^2E^2}{4H^2}\,a^4\varphi + m^2_{\rm ds}a^2\varphi = 0, \tag{4}$$

where the prime denotes a $\tau-$ derivative and the spatial index $i$ is summed over. The spatial translational invariance of Equation (4) suggests that we can consider

$$\varphi(\tau, \mathbf{x}) = a^{-1}(\tau)\phi_{\mathbf{k}}(\tau)\, e^{i\mathbf{k}\cdot\mathbf{x}}, \tag{5}$$

where, for the co-moving wave number $k^2 = k_x^2 + k_y^2 + k_z^2$, $\phi_{\mathbf{k}}(\tau)$ satisfies

$$\phi''_{\mathbf{k}\pm}(\tau) + \omega^2_{\mathbf{k}\pm}\, \phi_{\mathbf{k}\pm}(\tau) = 0, \tag{6}$$

with the effective frequency given by

$$\omega^2_{\mathbf{k}\pm} = k^2 + \frac{1}{\tau^2}\left(\frac{m^2_{\rm ds}}{H^2} - 2 \mp \frac{eE|k_z|}{H^3}\right) + \frac{e^2E^2}{4H^6\tau^4}\,. \tag{7}$$

Also, the subscripts $\pm$ correspond to the so-called "upward" ($k_z > 0$) and "downward" ($k_z < 0$) tunneling (or "anti-screening" and "screening" orientation), respectively.

From Equation (7), we observe that in the asymptotic past ($\tau \to +\infty$), we have $\omega_{\mathbf{k}\pm} \simeq k^2$ and thus $\phi_{\mathbf{k}\pm}(\tau)$ is a sum of plane waves. Indeed, at early times the adiabatic condition

$$\left(\frac{\omega'_{\mathbf{k}\pm}}{\omega^2_{\mathbf{k}\pm}}\right)^2 \ll 1, \qquad\qquad \frac{\omega''_{\mathbf{k}\pm}}{\omega^3_{\mathbf{k}\pm}} \ll 1, \tag{8}$$

is trivially satisfied, leading to a well-defined notion of adiabatic "*in*" vacuum. On the other hand, in the asymptotic future ($\tau \to 0$), the frequencies $\omega_{\mathbf{k}\pm}$ are determined by the last dominant term in Equation (7), i.e., $\omega_{\mathbf{k}\pm} \simeq \frac{e^2E^2}{4H^6\tau^4}$. Thus, in this case the adiabatic condition (8) is also well satisfied and then $\phi_{\mathbf{k}\pm}(\tau)$ is well approximated by a WKB solution in the asymptotic future. This means that there exists a well-defined adiabatic "*out*" vacuum. We employ these facts to compute the Bogoliubov coefficients and pair production in Section 4.

Introducing the dimensionless variable

$$\mathfrak{z} := -|k_z|\tau, \qquad\qquad \mathfrak{z} \in (0, +\infty),$$

Equation (6) can be recast as

$$\frac{\mathrm{d}^2}{\mathrm{d}\mathfrak{z}^2}\phi_{\mathbf{k}\pm}(\mathfrak{z}) + \left[\alpha - \frac{\tilde{\mu}^2 + \beta_\pm}{\mathfrak{z}^2} + \frac{\beta_\pm^2}{4\,\mathfrak{z}^4}\right]\phi_{\mathbf{k}\pm}(\mathfrak{z}) = 0, \tag{9}$$

where we have defined the dimensionless parameters

$$\mathcal{M} := \frac{m_{\rm ds}}{H}, \qquad \mathcal{E} := \frac{eE}{H^2}, \qquad \kappa_z := \frac{|k_z|}{H},$$
$$\alpha := \frac{k^2}{k_z^2} = 1 + \frac{k_x^2 + k_y^2}{k_z^2}, \qquad \beta_\pm := \pm\,\mathcal{E}\kappa_z, \qquad \tilde{\mu}^2 := 2 - \mathcal{M}^2.$$

To study the Schwinger effect, we need to solve this differential equation which has no exact solution. Therefore, one needs to resort to numerical or/and approximate methods. We will proceed to do this in the following sections.

## 3. Uniform Asymptotic Approximation and Mode Functions

To find the approximate analytical solution of Equation (9), we closely follow the approach of Refs. [41, 42, 43, 44], where the authors developed the *uniform asymptotic approximation method* for solving the second-order differential equation of the form $\mathrm{d}^2w/\mathrm{d}\mathfrak{z}^2 = \left[\lambda^2\hat{g}(\mathfrak{z}) + q(\mathfrak{z})\right] w$ that was originally formulated by Olver [26]. Here, we briefly apply this method to construct the solution and refer the reader to Refs. [24, 27, 28, 41, 42, 43, 44] for further details. To do this, we first rewrite Equation (9) in the form

$$\frac{\mathrm{d}^2}{\mathrm{d}\mathfrak{z}^2}\,\phi_{\mathbf{k}\pm}(\mathfrak{z}) = \left[\lambda^2\hat{g}(\mathfrak{z}) + q(\mathfrak{z})\right]\phi_{\mathbf{k}\pm}(\mathfrak{z}), \tag{10}$$

where

$$\lambda^2\hat{g}(\mathfrak{z}) + q(\mathfrak{z}) = -\left(\alpha - \frac{\tilde{\mu}^2+\beta_\pm}{\mathfrak{z}^2} + \frac{\beta_\pm^2}{4\,\mathfrak{z}^4}\right). \tag{11}$$

Here, $\lambda$ is a positive large parameter that is introduced to trace the order of the approximation and can be set to one at the end. The two functions $g(\mathfrak{z}) \equiv \lambda^2\hat{g}(\mathfrak{z})$ and $q(\mathfrak{z})$ cannot be uniquely determined from Equation (11). Nevertheless, as discussed in [27, 41, 42, 43, 44], they can be usually determined demanding that the associated errors of the approximate solutions are minimized. In view of (11), $\lambda^2\hat{g}(\mathfrak{z})$ and $q(\mathfrak{z})$ have a pole at $\mathfrak{z} = 0^+$ and $\lambda^2\hat{g}(\mathfrak{z})$ may vanish at the so-called *turning points* in the range $\mathfrak{z} \in (0^+, +\infty)$. The uniform asymptotic solutions of Equation (10) strictly depend on the nature of the turning points and the behavior of $\lambda^2\hat{g}(\mathfrak{z})$ and $q(\mathfrak{z})$ near the pole and turning points.

To specify the explicit form of $\lambda^2\hat{g}(\mathfrak{z})$ and $q(\mathfrak{z})$, we first apply the Liouville transformation with two new variables $\zeta(\mathfrak{z})$ and $U(\zeta)$, defined by [26, 27, 28]

$$U(\zeta) := \dot{\mathfrak{z}}^{-\frac{1}{2}}\phi(\mathfrak{z}), \qquad \dot{\mathfrak{z}}^{-2} := \left(\frac{\mathrm{d}\zeta}{\mathrm{d}\mathfrak{z}}\right)^2 = \frac{|\hat{g}(\mathfrak{z})|}{f^{(1)}(\zeta)^2}\,, \tag{12}$$

to Equation (10), where $f(\zeta) = \int \mathrm{d}\mathfrak{z}\sqrt{|\hat{g}(\mathfrak{z})|}$ and $f^{(1)}(\zeta) = \mathrm{d}f/\mathrm{d}\zeta$. This yields

$$\frac{\mathrm{d}^2U(\zeta)}{\mathrm{d}\zeta^2} = \left\{\pm\lambda^2 f^{(1)}(\zeta)^2 + \psi(\zeta)\right\}U(\zeta) \tag{13}$$

where

$$\psi(\zeta) = \dot{\mathfrak{z}}^2 q(\mathfrak{z}) + \dot{\mathfrak{z}}^{\frac{1}{2}}\frac{\mathrm{d}^2}{\mathrm{d}\zeta^2}(\dot{\mathfrak{z}}^{-\frac{1}{2}}) = \dot{\mathfrak{z}}^2 q(\mathfrak{z}) - \dot{\mathfrak{z}}^{\frac{3}{2}}\frac{\mathrm{d}^2}{\mathrm{d}\mathfrak{z}^2}(\dot{\mathfrak{z}}^{\frac{1}{2}}),$$

and $\pm$ correspond to $g(\mathfrak{z}) > 0$ and $g(\mathfrak{z}) < 0$, respectively. Clearly, the accuracy of the approximate solutions depends on the magnitude of $\psi(\zeta)$. As shown in [28, 41, 42, 43, 44], the errors of the approximate solutions are characterized by an error control function, $\mathcal{F}(\mathfrak{z})$, that in the first-order, with the choice of $f^{(1)}(\zeta)^2 = 1$, is defined by

$$\mathcal{F}(\mathfrak{z}) = \int \mathrm{d}\mathfrak{z}\,|\psi(\mathfrak{z})| = \int \mathrm{d}\mathfrak{z}\left\{\frac{5}{16}\frac{g'^2(\mathfrak{z})}{g^{5/2}(\mathfrak{z})} - \frac{1}{4}\frac{g''(\mathfrak{z})}{g^{3/2}(\mathfrak{z})} - \frac{q(\mathfrak{z})}{g^{1/2}(\mathfrak{z})}\right\}. \tag{14}$$

As pointed out in [41, 42, 43, 44], the Liouville-Green approximation is valid provided that, near the pole $\mathfrak{z} = 0^+$ the two conditions hold: $(i)$ $|\lambda^2\hat{g}(\mathfrak{z})| \ll |q(\mathfrak{z})|$ everywhere, except in the neighborhood of turning points, and $(ii)$ the error control function $\mathcal{F}(\mathfrak{z})$ must be finite (convergent). Assuming that $\lambda^2\hat{g}(\mathfrak{z})$ and $q(\mathfrak{z})$ have a pole at $\mathfrak{z} = 0^+$, respectively, of order $i$ and $j$, one can expand them in the region near the pole $\mathfrak{z} = 0^+$ in the form

$$\lambda^2\hat{g}(\mathfrak{z}) = \frac{1}{\mathfrak{z}^i}\sum_{s=0}^{\infty} g_s\mathfrak{z}^s, \qquad\qquad q(\mathfrak{z}) = \frac{1}{\mathfrak{z}^j}\sum_{s=0}^{\infty} q_s\mathfrak{z}^s,$$

where $g_s$ and $q_s$ are some constants. Making use of these expansion in (14), at the leading order we find

$$\mathcal{F}(\mathfrak{z}) \simeq -g_0^{-\frac{1}{2}}\int \mathrm{d}\mathfrak{z}\left\{q_0\,\mathfrak{z}^{\frac{i}{2}-j} + \left(\frac{i(i+1)}{4} - \frac{5\,i^2}{16}\right)\mathfrak{z}^{\frac{i}{2}-2}\right\}.$$

In view of (11), when $\beta_\pm \neq 0$, the condition $(i)$ requires that $\lambda^2\hat{g}(\mathfrak{z})$ must be of order $i = 4$ at the pole $\mathfrak{z} = 0^+$, while $q(\mathfrak{z})$ can be of order $j \leq 3$. However, for the case $\beta_\pm = 0$, we have $i = j = 2$ (see [41, 42, 43, 44] for details). Therefore, in this case, to keep $\mathcal{F}(\mathfrak{z})$ finite near the pole, we must choose $q_0 = -1/4$. On the other hand, we must set $q_s = 0$ for $s \geq 1$ to ensure that the condition $|\lambda^2\hat{g}(\mathfrak{z})| \ll |q(\mathfrak{z})|$ holds. This implies $q(\mathfrak{z}) = -\frac{1}{4\,\mathfrak{z}^2}$, which, in view of (11), results in

$$\lambda^2\hat{g}(\mathfrak{z}) = -\left(\alpha - \frac{\mu^2+\beta_\pm}{\mathfrak{z}^2} + \frac{\beta_\pm^2}{4\,\mathfrak{z}^4}\right), \tag{15}$$

with $\mu^2 := \tilde{\mu}^2 + \frac{1}{4} = \frac{9}{4} - \mathcal{M}^2$.

## 3.1 Turning Points

Having determined the function $\lambda^2\hat{g}(\mathfrak{z})$, now we are ready to find its turning points. These are the zeros of the equation $\lambda^2\hat{g}(\mathfrak{z}) = 0$ that can be cast in the form

$$4\alpha\,\mathfrak{z}^4 - 4(\mu^2+\beta_\pm)\,\mathfrak{z}^2 + \beta_\pm^2 = 0.$$

This is a quartic equation which can have at most four roots. Its discriminant

$$\Delta = 4^7\alpha\beta_\pm^2\left((\mu^2+\beta_\pm)^2 - \alpha\beta_\pm^2\right)^2,$$

is always non-negative and depending on the values of $\alpha$, $\mu^2$ and $\beta_\pm$ the nature of the four roots is different. There are four different cases to consider.

$(a)$ When $0 \leq \mathcal{M}^2 < \frac{9}{4} - (\sqrt{\alpha}\mp 1)|\beta_\pm|$, we have $\mu^2+\beta_\pm > 0$, $(\mu^2+\beta_\pm)^2 - \alpha\beta_\pm^2 > 0$, and hence $\Delta > 0$, such that there are four distinct real roots. But we have two real turning points $\mathfrak{z}_{1\pm} < \mathfrak{z}_{2\pm}$ in the interval $(0, +\infty)$ which are given by

$$\mathfrak{z}_{i\pm} = \frac{1}{\sqrt{2\alpha}}\Big((\mu^2+\beta_\pm) + \epsilon_i\sqrt{(\mu^2+\beta_\pm)^2 - \alpha\beta_\pm^2}\,\Big)^{1/2}, \tag{16}$$

where $\epsilon_1 = -1$ and $\epsilon_2 = +1$.

($b$) When $\frac{9}{4} - (\sqrt{\alpha} \mp 1)|\beta_\pm| < \mathcal{M}^2 < \frac{9}{4} + (\sqrt{\alpha} \pm 1)|\beta_\pm|$, we have $\Delta > 0$, but $\mu^2 + \beta_\pm$ may be positive, negative or zero. In this case, there are two pairs of non-real complex conjugate roots which one of them with the positive real part to be considered here. These are

$$\mathfrak{z}_{1\pm} = \frac{\sqrt{|\beta_\pm|}}{\sqrt{2}\,\alpha^{1/4}} \Big\{ \cos(\vartheta_\pm/2) - i \sin(\vartheta_\pm/2) \Big\} = \mathfrak{z}_{2\pm}^*, \tag{17}$$

where $\vartheta_\pm$ is defined by

$$\vartheta_\pm = \arccos\left( \frac{\mu^2 + \beta_\pm}{|\beta_\pm|\sqrt{\alpha}} \right).$$

($c$) When $\mathcal{M}^2 = \frac{9}{4} - (\sqrt{\alpha} \mp 1)|\beta_\pm|$ or $\mathcal{M}^2 = \frac{9}{4} + (\sqrt{\alpha} \pm 1)|\beta_\pm|$, we have $\Delta = 0$ and there are two real or purely imaginary double roots depending on whether $\mu^2 + \beta_\pm$ is positive or negative, respectively. The acceptable double root in each case is $\mathfrak{z}_\pm = \sqrt{(\mu^2 + \beta_\pm)/2\alpha}$.

($d$) When $\mathcal{M}^2 > \frac{9}{4} + (\sqrt{\alpha} \pm 1)|\beta_\pm|$, we have $\Delta > 0$, but $\mu^2 + \beta_\pm$ is negative and there are two pairs of purely imaginary complex conjugate roots given by

$$\mathfrak{z}_{i\pm} = \frac{i}{\sqrt{2\alpha}} \Big( |\mu^2 + \beta_\pm| + \epsilon_i \sqrt{(\mu^2 + \beta_\pm)^2 - \alpha\beta_\pm^2} \Big)^{1/2},$$

and their complex conjugates.

Thus, for the cases of small masses, weak electric fields and small momentums, we have two real turning points $\mathfrak{z}_{1\pm} < \mathfrak{z}_{2\pm}$. The case of two complex conjugate turning points $\mathfrak{z}_{1\pm} = \mathfrak{z}_{2\pm}^*$ occurs when we have moderate to large masses, moderate to strong electric fields or large momentums. Double turning points (real or purely imaginary) can be obtained by the fine-tuning of the free parameters involved in the theory, i.e., $E$, $m$, and $\mathbf{k}$. Finally, very heavy particles (masses) (compared to the electric field and momentum) lead to four purely imaginary turning points. Physically, heavy particles are hard to be produced, so therefore we did not consider this case, i.e., ($d$), in the following.

## 3.2 Approximate Solutions Near the Pole $\mathfrak{z} = 0^+$ and Two Turning Points $\mathfrak{z}_1$ and $\mathfrak{z}_2$

Finally, as shown in [26, 41, 42, 43, 44], we find that the approximate solutions and the corresponding error bounds near the pole $\mathfrak{z} = 0^+$ and around the turning points can be constructed as follows. The approximate solution near the pole $\mathfrak{z} = 0^+$ can be obtained by choosing $f^{(1)}(\zeta)^2 = \text{const} = 1$. Because $g(\mathfrak{z})$ is negative near the pole, we then find from (13) that $\mathrm{d}^2U/\mathrm{d}\zeta^2 = \big[-\lambda^2 + \psi(\zeta)\big]\,U$, where $U(\zeta) = (-g(\mathfrak{z}))^{1/4}\phi(\mathfrak{z})$ and $\zeta(\mathfrak{z}) = \int^{\mathfrak{z}} \mathrm{d}\mathfrak{z}' \sqrt{-\hat{g}(\mathfrak{z}')}$. Therefore, neglecting the $\psi(\zeta)$

term, to first-order approximation, $\phi_{\mathbf{k}\pm}(\mathfrak{z})$ near the pole $\mathfrak{z} = 0^+$ is given by the Liouville-Green approximate solution

$$\phi_{\mathbf{k}\pm}(\mathfrak{z}) = \frac{c_1}{(-\hat{g}(\mathfrak{z}))^{\frac{1}{4}}}\, e^{i\lambda\int^{\mathfrak{z}}\mathrm{d}\mathfrak{z}'\sqrt{-\hat{g}(\mathfrak{z}')}}(1+\epsilon_1)+\frac{c_2}{(-\hat{g}(\mathfrak{z}))^{\frac{1}{4}}}\, e^{-i\lambda\int^{\mathfrak{z}}\mathrm{d}\mathfrak{z}'\sqrt{-\hat{g}(\mathfrak{z}')}}(1+\epsilon_2), \quad (18)$$

where $c_1$ and $c_2$ are integration constants, and $\epsilon_1$ and $\epsilon_2$ denote the errors of the approximate solution whose definition can be found in Refs. [28, 41, 42, 43, 44].

As pointed out in [26, 41, 42, 43, 44], the crucial point to get the asymptotic solution near two turning points $\mathfrak{z}_1$ and $\mathfrak{z}_2$ is to choose $f^{(1)}(\zeta)^2 = |\zeta^2 - \zeta_0^2|$ in Equation (12), where $\zeta$ is an increasing function of $\mathfrak{z}$ with the conditions $\zeta(\mathfrak{z}_1) = -\zeta_0$ and $\zeta(\mathfrak{z}_2) = \zeta_0$. In this case, Equation (13) reduces to $\mathrm{d}^2U/\mathrm{d}\zeta^2 = \left[\lambda^2(\zeta_0^2 - \zeta^2) + \psi(\zeta)\right]U$. Ignoring the term $\psi(\zeta)$, the first-order solution to this so-called *Weber equation* can be expressed in terms of the *parabolic cylinder functions* $D_\nu(\sqrt{2\lambda}\zeta\, e^{-i\frac{\pi}{4}})$ and $D_{-\nu-1}(\sqrt{2\lambda}\zeta\, e^{i\frac{\pi}{4}})$ [28, 40], where $\nu$ is defined by (see Appendix for details)

$$\nu := -\frac{1}{2} - \frac{i}{2}\lambda\zeta_0^2.$$

Thus, the general first-order approximate solution of Equation (9) near two turning points $\mathfrak{z}_1$ and $\mathfrak{z}_2$ is given by

$$\phi_{\mathbf{k}\pm}(\mathfrak{z}) = \left(\frac{\zeta^2 - \zeta_0^2}{-\hat{g}(\mathfrak{z})}\right)^{1/4}\left[C_1 D_\nu(\sqrt{2\lambda}\zeta\, e^{-i\pi/4}) + C_2 D_{-\nu-1}(\sqrt{2\lambda}\zeta\, e^{i\pi/4})\right], \quad (19)$$

where $C_1$ and $C_2$ are two integration constants and we have omitted the error terms. The relation between $\zeta(\mathfrak{z})$ and $\mathfrak{z}$ can be easily derived from Equation (12). Consider that $\mathfrak{z}_1$ and $\mathfrak{z}_2$ ($\mathfrak{z}_1 < \mathfrak{z}_2$) are real turning points. When $\mathfrak{z} < \mathfrak{z}_1$, one has $\zeta < -\zeta_0$ and $g(\mathfrak{z}) < 0$ which imply

$$\int_{\mathfrak{z}_1}^{\mathfrak{z}} \mathrm{d}\mathfrak{z}'\sqrt{-g(\mathfrak{z}')} = \frac{1}{2}\zeta\sqrt{\zeta^2 - \zeta_0^2} + \frac{1}{2}\zeta_0^2\,\mathrm{arccosh}(-\zeta/\zeta_0).$$

When $\mathfrak{z} > \mathfrak{z}_2$, one has $\zeta > \zeta_0$ and $g(\zeta) < 0$ which yield

$$\int_{\mathfrak{z}_2}^{\mathfrak{z}} \mathrm{d}\mathfrak{z}'\sqrt{-g(\mathfrak{z}')} = \frac{1}{2}\zeta\sqrt{\zeta^2 - \zeta_0^2} - \frac{1}{2}\zeta_0^2\,\mathrm{arccosh}(\zeta/\zeta_0).$$

And in the region $\mathfrak{z}_1 \le \mathfrak{z} \le \mathfrak{z}_2$, one has $-\zeta_0 \le \zeta \le \zeta_0$ and $g(\mathfrak{z}) > 0$ which result in

$$\int_{\mathfrak{z}_1}^{\mathfrak{z}} \mathrm{d}\mathfrak{z}'\sqrt{g(\mathfrak{z}')} = \frac{1}{2}\zeta\sqrt{\zeta_0^2 - \zeta^2} + \frac{1}{2}\zeta_0^2\,\arccos(-\zeta/\zeta_0).$$

Note that in the above relation, if we take the upper limit of the integral to be $\mathfrak{z}_2$, we obtain

$$\zeta_0^2 = \frac{2}{\pi}\int_{\mathfrak{z}_1}^{\mathfrak{z}_2} \mathrm{d}\mathfrak{z}\sqrt{\hat{g}(\mathfrak{z})}. \quad (20)$$

Finally, we recall from [41, 42, 43, 44] that the general approximate solution (19) is valid when $\mathfrak{z}_1$ and $\mathfrak{z}_2$ are two complex turning points. But it should be noted that in this case $\zeta_0^2$ is always negative ($\zeta_0$ is purely imaginary), and thus the relation between $\zeta(\mathfrak{z})$ and $\mathfrak{z}$ is given by

$$\int_{\Re(\mathfrak{z}_1)}^{\mathfrak{z}} \mathrm{d}\mathfrak{z}' \sqrt{-g(\mathfrak{z}')} = \frac{1}{2}\zeta\sqrt{\zeta^2-\zeta_0^2} - \frac{1}{2}\zeta_0^2 \operatorname{arcsinh}(\zeta/|\zeta_0|),$$

where $\Re$ stands for "*the real part of*".

We close this section to comment on the validity of the first-order approximation used to derive the approximate solutions. In the next section, we will use the physically well-defined initial conditions to determine the integration constants $C_1$ and $C_2$. The analytical approximate solution (19) with $C_1$ and $C_2$ being given by Equation (23) is compared with the numerical solution in Figures 1 (for $k_z > 0$) and 2 (for $k_z < 0$). These figures and many other ones we examined show that the exact solution of Equation (9) are well approximated by our first-order approximate analytical solution (19). In the next section we will also observe that the pair production probability obtained by these approximate solutions is very close to the numerical (exact) value. These observations show that the first-order approximation works well and there is no need to extend the solution (19) to high orders.

# 4. Pair Production Probability

Having obtained the general approximate solutions, let us compute the Schwinger pair production. To do this end, we need to specify the positive- and negative-frequency mode functions that define the so-called *in* and *out* vacua.

As pointed out in Section 2, there exist adiabatic in and out vacua corresponding, respectively, to the plane wave and WKB solutions in the asymptotic past and future. Therefore, at early times $\tau \to -\infty$ ($\mathfrak{z} \to +\infty$), for which we have $\lambda^2\hat{g}(\mathfrak{z}) \simeq -\alpha$, we choose the normalized positive-frequency solutions $\phi_{\mathbf{k}\pm}^{(\mathrm{in},+)}(\mathfrak{z})$ to have the asymptotic form

$$\lim_{\mathfrak{z}\to+\infty} \phi_{\mathbf{k}\pm}^{(\mathrm{in},+)}(\mathfrak{z}) = \frac{e^{i\sqrt{\alpha}\,\mathfrak{z}}}{\sqrt{2|k_z|}\,\alpha^{1/4}}\,. \tag{21}$$

Considering the asymptotic form of the parabolic cylinder functions in the limit $\mathfrak{z} \to +\infty$ ($\zeta \to +\infty$) given by Equations (34) and (35), the general approximate solution (19) take the asymptotic form

$$\phi_{\mathbf{k}\pm}(\mathfrak{z}) \simeq (-2\lambda\hat{g}(\mathfrak{z}))^{-\frac{1}{4}}\, e^{-\frac{\pi}{8}\lambda\zeta_0^2}\left[C_1 e^{i\chi(\mathfrak{z})} + C_2 e^{-i\chi(\mathfrak{z})}\right], \tag{22}$$

where, with $\phi_2 := \mathrm{ph}\,\Gamma\big(\frac{1}{2} + \frac{i}{2}\lambda\zeta_0^2\big)$, the function $\chi(\mathfrak{z})$ is defined by

$$\chi(\mathfrak{z}) := \int_{\mathfrak{z}_2}^{\mathfrak{z}} \sqrt{-g(\mathfrak{z}')}\,\mathrm{d}\mathfrak{z}' + \frac{\pi}{8} - \frac{1}{2}\phi_2\,.$$

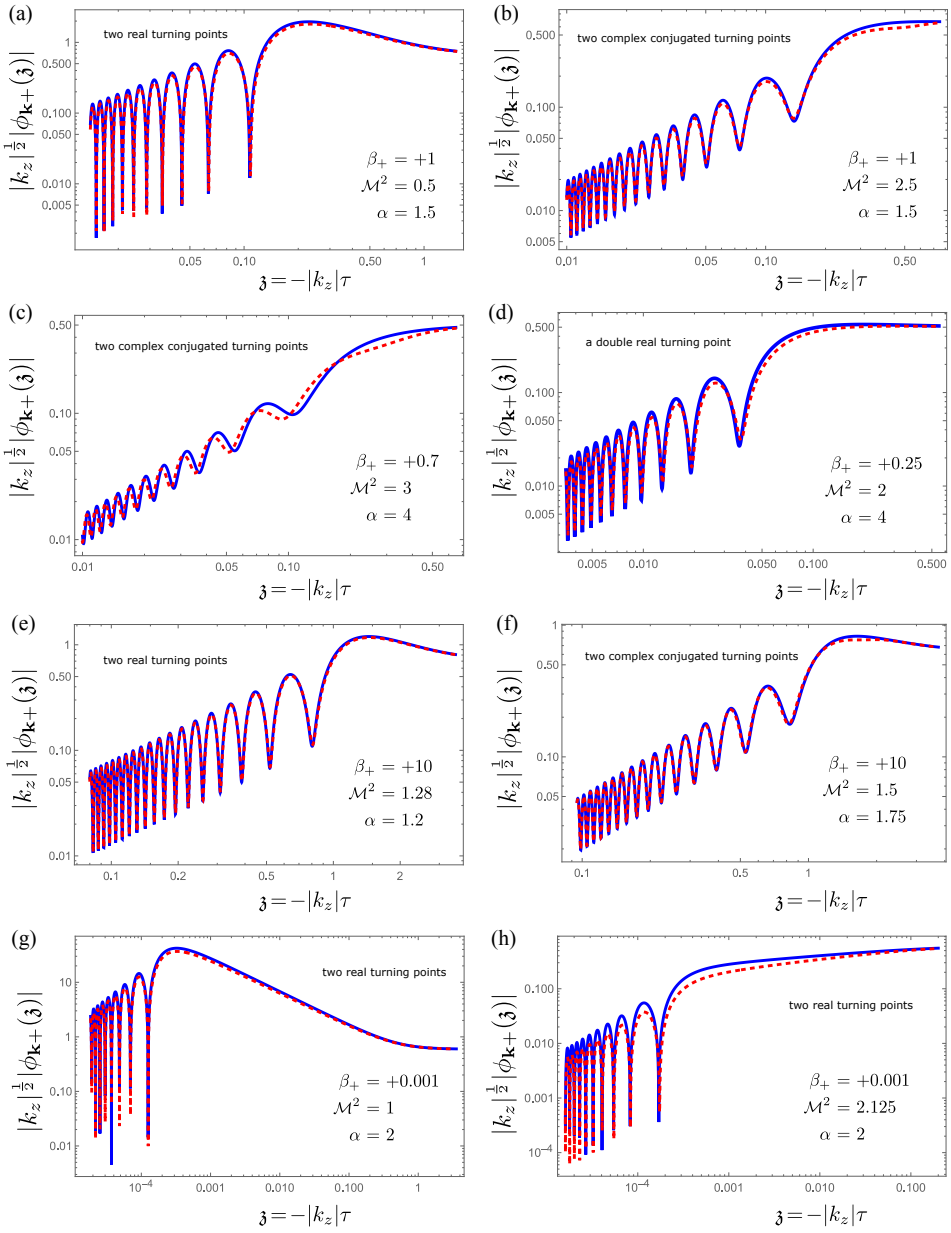


Figure 1: Comparison between the numerical (exact) (blue solid curves) and approximate analytical (red dotted curves) mode functions $\phi_{\mathbf{k}+}(\mathfrak{z})$ for $k_z > 0$. The figures (a), (e), (g) and (h) correspond to case $(a)$ with two real turning points, while (b), (c) and (f) correspond to case $(b)$ with two complex conjugated turning points. The panel (d) corresponds to case $(c)$ with a double real turning point.

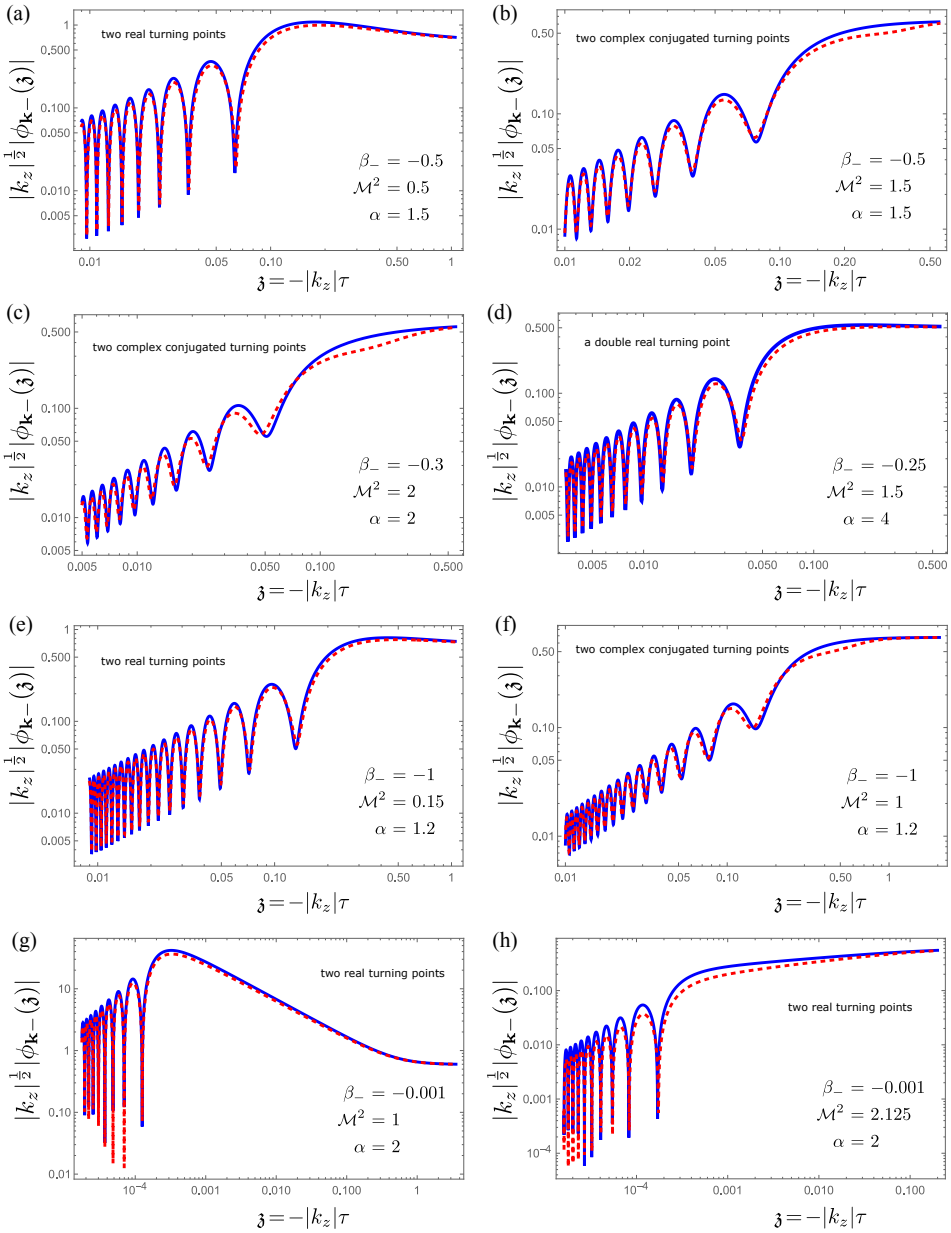


Figure 2: Comparison between the numerical (exact) (blue solid curves) and approximate analytical (red dotted curves) mode functions $\phi_{\mathbf{k}-}(\mathfrak{z})$ for $k_z < 0$. The figures (a), (e), (g) and (h) correspond to case $(a)$ with two real turning points, while (b), (c) and (f) correspond to case $(b)$ with two complex conjugated turning points. The panel (d) corresponds to case $(c)$ with a double real turning point.

Making use of $g(\mathfrak{z}) \to -\alpha$ in the limit $\mathfrak{z} \to +\infty$, one can easily see that the right-hand side of Equation (22) can be matched with the expression (21) if, up to an irrelevant phase factor, we set

$$C_1 = (2\lambda|k_z|^2)^{-1/4}\, e^{\frac{\pi}{8}\lambda\zeta_0^2}, \qquad\qquad C_2 = 0. \tag{23}$$

In light of (5) and (19), these integration constants imply that

$$\begin{aligned}\varphi^{(\mathrm{in},+)}_{\mathbf{k}\pm}(x) \;&=\; a^{-1}(\tau) e^{i\mathbf{k}\cdot\mathbf{x}} \phi^{(\mathrm{in},+)}_{\mathbf{k}\pm}(\tau)\\ &=\; a^{-1}(\tau)\, e^{i\mathbf{k}\cdot\mathbf{x}} |k_z|^{-\frac{1}{2}} e^{\frac{\pi}{8}\lambda\zeta_0^2} \left(\frac{\zeta^2-\zeta_0^2}{-2\lambda\hat{g}(\mathfrak{z})}\right)^{\frac{1}{4}} D_\nu(\sqrt{2\lambda}\zeta\, e^{-i\pi/4})\end{aligned} \tag{24}$$

describes the positive-frequency mode function for the in vacuum. Similarly, the negative-frequency mode function for the in vacuum can be obtained by $C_1 = 0$ and $C_2 = (2\lambda|k_z|^2)^{-1/4}\, e^{\frac{\pi}{8}\lambda\zeta_0^2}$, i.e., we have

$$\varphi^{(\mathrm{in},-)}_{\mathbf{k}\pm}(x) = a^{-1}(\tau)\, e^{-i\mathbf{k}\cdot\mathbf{x}} |k_z|^{-\frac{1}{2}} e^{\frac{\pi}{8}\lambda\zeta_0^2} \left(\frac{\zeta^2-\zeta_0^2}{-2\lambda\hat{g}(\mathfrak{z})}\right)^{\frac{1}{4}} D_{-\nu-1}(\sqrt{2\lambda}\zeta\, e^{i\pi/4}). \tag{25}$$

At late times $\tau \to 0^-$ ($\mathfrak{z} \to 0^+$) the positive-frequency solution of Equation (9) should asymptotically take the form of the WKB solution

$$\phi^{(\mathrm{out},+)}_{\mathbf{k}\pm}(\mathfrak{z}) = \frac{1}{\sqrt{2\,\omega_{k\pm}}}\, e^{-i\int \omega_{k\pm}\mathrm{d}\tau} \simeq \frac{1}{\sqrt{2|k_z|}(-g(\mathfrak{z}))^{\frac{1}{4}}} \exp\left[i\int^{\mathfrak{z}} \mathrm{d}\mathfrak{z}'\sqrt{-g(\mathfrak{z}')}\right]. \tag{26}$$

The Liouville-Green approximate solution (18) near the pole $\mathfrak{z} = 0^+$ matches with the WKB solution (26) if, up to an irrelevant phase factor, we set $c_1 = (2\lambda|k_z|)^{-1/2}$ and $c_2 = 0$. On the other hand, the negative-frequency solution is simply given by the choice $c_1 = 0$ and $c_2 = (2\lambda|k_z|)^{-1/2}$. Thus, the positive- and negative-frequency mode functions for the out vacuum can be expressed by

$$\begin{aligned}\varphi^{(\mathrm{out},+)}_{\mathbf{k}\pm}(x) \;&=\; a^{-1}(\tau) e^{i\mathbf{k}\cdot\mathbf{x}} \phi^{(\mathrm{out},+)}_{\mathbf{k}\pm}(\tau)\\ &=\; \frac{a^{-1}(\tau)\, e^{i\mathbf{k}\cdot\mathbf{x}}}{\sqrt{2|k_z|}(-g(\mathfrak{z}))^{\frac{1}{4}}} \exp\left[i\int^{\mathfrak{z}} \mathrm{d}\mathfrak{z}'\sqrt{-g(\mathfrak{z}')}\right],\end{aligned} \tag{27}$$

and $\varphi^{(\mathrm{out},-)}_{\mathbf{k}\pm}(x) = \varphi^{(\mathrm{out},+)}_{\mathbf{k}\pm}(x)^*$.

Having determined the in and out mode functions (given by Equations (24), (25) and (27)), we can compute the Bogoliubov coefficients. To do this, we use the asymptotic form of $\varphi^{(\mathrm{in},+)}_{\mathbf{k}\pm}(x)$ in the infinite future $\tau \to 0^-$ ($\mathfrak{z} \to 0^+$ or $\zeta \to -\infty$). In view of the asymptotic relation (37), and Equation (27), in this limit we have

$$\begin{aligned}\lim_{\mathfrak{z}\to 0^+} \phi^{(\mathrm{in},+)}_{\mathbf{k}\pm}(\mathfrak{z}) &= \lim_{\zeta\to-\infty} |k_z|^{-\frac{1}{2}} e^{\frac{\pi}{8}\lambda\zeta_0^2} \left(\frac{\zeta^2-\zeta_0^2}{-2\lambda\hat{g}(\mathfrak{z})}\right)^{\frac{1}{4}} D_\nu(\sqrt{2\lambda}\zeta\, e^{-i\pi/4})\\ &\simeq \frac{e^{i(\frac{\pi}{8}-\frac{1}{2}\phi_2)}}{\sqrt{2|k_z|}\,(-g(\mathfrak{z}))^{\frac{1}{4}}} \left[\sqrt{1+e^{\pi\lambda\zeta_0^2}} e^{-i\tilde{\chi}(\mathfrak{z})} - ie^{\frac{\pi}{2}\lambda\zeta_0^2} e^{i\tilde{\chi}(\mathfrak{z})}\right]\\ &= e^{i(\frac{\pi}{8}-\frac{1}{2}\phi_2)} \left[\sqrt{1+e^{\pi\lambda\zeta_0^2}}\,\phi^{(\mathrm{out},+)}_{\mathbf{k}\pm}(\mathfrak{z}) - ie^{\frac{\pi}{2}\lambda\zeta_0^2}\phi^{(\mathrm{out},-)}_{\mathbf{k}\pm}(\mathfrak{z})\right],\end{aligned}$$

where in second line we used the notation $\tilde{\chi}(\mathfrak{z}) := -\int_{\mathfrak{z}_1}^{\mathfrak{z}} \sqrt{-g(\mathfrak{z}')}\,\mathrm{d}\mathfrak{z}'$. This, in turn, implies that

$$\varphi^{(\mathrm{in},+)}_{\mathbf{k}\pm}(x) \simeq \int \frac{\mathrm{d}^3\mathbf{k}'}{(2\pi)^3}\left(\alpha_{\mathbf{k}\pm,\mathbf{k}'}\varphi^{(\mathrm{out},+)}_{\mathbf{k}'\pm}(x) + \beta_{\mathbf{k}\pm,\mathbf{k}'}\varphi^{(\mathrm{out},-)}_{\mathbf{k}'\pm}(x)\right),$$

where the Bogoliubov coefficients $\alpha_{\mathbf{k}\pm,\mathbf{k}'}$ and $\beta_{\mathbf{k}\pm,\mathbf{k}'}$ are given by

$$\begin{aligned} \alpha_{\mathbf{k}\pm,\mathbf{k}'} &= (2\pi)^3\delta^3(\mathbf{k}-\mathbf{k}')\alpha_{\mathbf{k}\pm}, & \alpha_{\mathbf{k}\pm} &= \sqrt{1+e^{\pi\lambda\zeta_0^2}},\\ \beta_{\mathbf{k}\pm,\mathbf{k}'} &= (2\pi)^3\delta^3(\mathbf{k}+\mathbf{k}')\beta_{\mathbf{k}\pm}, & \beta_{\mathbf{k}\pm} &= ie^{\frac{\pi}{2}\lambda\zeta_0^2}. \end{aligned} \tag{28}$$

Here we have ignored the unphysical global phase factor $e^{i(\frac{\pi}{8}-\frac{1}{2}\phi_2)}$. These Bogoliubov coefficients explicitly satisfy the normalization condition $|\alpha_{\mathbf{k}\pm}|^2-|\beta_{\mathbf{k}\pm}|^2=1$.

Now we are in a position to compute the probability of pair production. The in and out vacua are respectively defined by $a_{\mathrm{out}\mathbf{k}}|0\rangle_{\mathrm{out}} = b_{\mathrm{out}\mathbf{k}}|0\rangle_{\mathrm{out}} = 0$ and $a_{\mathrm{in}\mathbf{k}}|0\rangle_{\mathrm{in}} = b_{\mathrm{in}\mathbf{k}}|0\rangle_{\mathrm{in}} = 0$, for all $\mathbf{k}$, where the late time annihilation operators $a_{\mathrm{out}\mathbf{k}}$ and $b_{\mathrm{out}\mathbf{k}}$ are related to the early time creation and annihilations operators by a Bogoliubov transformation [29]

$$a_{\mathrm{out}\mathbf{k}} = \alpha_{\mathbf{k}}\, a_{\mathrm{in}\mathbf{k}} + \beta^*_{\mathbf{k}}\, b^\dagger_{\mathrm{in}-\mathbf{k}}\,, \qquad\qquad b_{\mathrm{out}\mathbf{k}} = \beta^*_{-\mathbf{k}}\, a^\dagger_{\mathrm{in}-\mathbf{k}} + \alpha_{-\mathbf{k}}\, b_{\mathrm{in}\mathbf{k}}.$$

In view of this transformation, and Equation (28), for each comoving wave vector $\mathbf{k}$ (with positive or negative $k_z$), the number of created pairs in the out vacuum $|0\rangle_{\mathrm{out}}$ per comoving three-volume is simply given by

$$\frac{{}_{\mathrm{out}}\langle 0|a^\dagger_{\mathrm{in}\mathbf{k}}a_{\mathrm{in}\mathbf{k}}|0\rangle_{\mathrm{out}}}{(2\pi)^3\int \mathrm{d}^3\mathbf{x}} = \frac{{}_{\mathrm{out}}\langle 0|b^\dagger_{\mathrm{in}-\mathbf{k}}b_{\mathrm{in}-\mathbf{k}}|0\rangle_{\mathrm{out}}}{(2\pi)^3\int \mathrm{d}^3\mathbf{x}} = \frac{|\beta_{\mathbf{k}\pm}|^2}{(2\pi)^3} = \frac{e^{\pi\lambda\zeta_0^2}}{(2\pi)^3}\,.$$

Therefore, the nature of the particle creation effect in the background potential (3) can be characterized by the quantity $\zeta_0^2$. The nature and value of $\zeta_0^2$, and therefore the behavior of pair creation strictly depends on the nature of two turning points $\mathfrak{z}_1$ and $\mathfrak{z}_2$. In the following we treat this issue for three different cases of turning points considered in section 3.

**Case (*a*)** $0 \le \mathcal{M}^2 < \frac{9}{4} - (\sqrt{\alpha}\mp 1)|\beta_\pm|$ **:** In this case, to calculate $\lambda\zeta_0^2$, we use Equations (20) and (15) to write

$$\lambda\zeta_0^2 = \frac{2}{\pi}\int_{\mathfrak{z}_{1\pm}}^{\mathfrak{z}_{2\pm}} \mathrm{d}\mathfrak{z}\sqrt{g(\mathfrak{z})} = \frac{2\sqrt{\alpha}}{\pi}\int_{\mathfrak{z}_{1\pm}}^{\mathfrak{z}_{2\pm}} \frac{\mathrm{d}\mathfrak{z}}{\mathfrak{z}^2}\sqrt{(\mathfrak{z}^2-\mathfrak{z}_{1\pm}^2)(\mathfrak{z}_{2\pm}^2-\mathfrak{z}^2)}\,, \tag{29}$$

where $\mathfrak{z}_{1\pm}$ and $\mathfrak{z}_{2\pm}$ are two real turning points given in (16). The integral can be performed by the change of variable $\mathfrak{z}^2 = \mathfrak{z}_{2\pm}^2 - (\mathfrak{z}_{2\pm}^2-\mathfrak{z}_{1\pm}^2)\sin^2\theta$. A part-by-part integration then yields

$$\lambda\zeta_0^2 = \frac{2}{\pi}\sqrt{\alpha}\,\mathfrak{z}_{2\pm}\Big(1-\frac{\mathfrak{z}_{1\pm}^2}{\mathfrak{z}_{2\pm}^2}\Big)\int_0^{\frac{\pi}{2}}\mathrm{d}\theta\,\frac{2\sin^2\theta-1}{\sqrt{1-\big(1-\mathfrak{z}_{1\pm}^2/\mathfrak{z}_{2\pm}^2\big)\sin^2\theta}}\,,$$

that can be expressed in terms of the complete elliptic integrals of the first and second kinds $K(\mathfrak{m})$ and $E(\mathfrak{m})$ [13, 28]. The result is

$$\pi\lambda\zeta_0^2 = 4\sqrt{\alpha}\,\mathfrak{z}_{2\pm}\left[\left(1-\frac{\mathfrak{m}^2}{2}\right)K(\mathfrak{m})-E(\mathfrak{m})\right], \tag{30}$$

where (here $0<\mathfrak{m}\leq 1$)

$$\mathfrak{m} := \sqrt{1-\mathfrak{z}_{1\pm}^2/\mathfrak{z}_{2\pm}^2} = \sqrt{2}\Big[1+\Big(1-\frac{\alpha\beta_\pm^2}{(\mu^2+\beta_\pm)^2}\Big)^{-\frac{1}{2}}\Big]^{-\frac{1}{2}}.$$

is the *modulus* of the elliptic functions. The result (30) (more precisely, the pair production probability $|\beta_{\mathbf{k}\pm}|^2 = e^{\pi\lambda\zeta_0^2}$) is compared with the numerical one in Figures 3 (for $k_z>0$) and 4 (for $k_z<0$). As can be seen from these plots, the more smaller the pair's mass and momentum are the easier it to be created by the Schwinger mechanism (remember that $\beta_\pm$ linearly depends on $k_z$). Also, comparing figures 3 and 4 show that the modes with anti-screening orientations ($k_z>0$) are hardest to be produced than those with screening ($k_z<0$) orientations.

**Case (*b*)** $\frac{9}{4}-(\sqrt{\alpha}\mp 1)|\beta_\pm| < \mathcal{M}^2 < \frac{9}{4}+(\sqrt{\alpha}\pm 1)|\beta_\pm|$**:** In this case, $\lambda\zeta_0^2 = 2\pi^{-1}\int_{\mathfrak{z}_{1\pm}}^{\mathfrak{z}_{2\pm}}\mathrm{d}\mathfrak{z}\sqrt{-g(\mathfrak{z})}$ can be expressed by a similar expression as in (29) in which $\mathfrak{z}_{1\pm}$ and $\mathfrak{z}_{2\pm}$ stands for the pair of complex conjugate turning points given by Equation (17). Noting that the path of integration lies along the imaginary axis, we can use $\mathfrak{z}=\Re(\mathfrak{z}_{1\pm})+is$ to perform the integral over $s$ from $\Im(\mathfrak{z}_{1\pm})$ to $\Im(\mathfrak{z}_{2\pm})$, where $\Im$ stands for '*the imaginary part of*'. The result is

$$\begin{aligned}\pi\lambda\zeta_0^2 \;=\; 4\sqrt{\alpha}\,\Im\Big[\mathfrak{z}_{1\pm}\Big\{&2\big(E(\mathfrak{n})-E(\psi,\mathfrak{n})\big)+(\mathfrak{n}^2-1)\big(K(\mathfrak{n})-F(\psi,\mathfrak{n})\big)\\ &+i(\mathfrak{n}-1)\sqrt{1-\big(1-2(\mathfrak{n}+1)^{-1}\big)^2/4}\Big\}\Big],\end{aligned} \tag{31}$$

where $F(\psi,\mathfrak{n})$ and $E(\psi,\mathfrak{n})$ denote the elliptic integrals of the first and second kind [13, 28], whose argument $\psi$ and modulus $\mathfrak{n}$ are defined by

$$\psi := \arcsin\Big(\frac{1}{2}(1+\mathfrak{n}^{-1})\Big), \qquad\qquad \mathfrak{n} := \frac{\mathfrak{z}_{2\pm}}{\mathfrak{z}_{1\pm}} = e^{i\vartheta_\pm}.$$

The result (31) for $\lambda\zeta_0^2$ and the corresponding approximate pair production probability $e^{\pi\lambda\zeta_0^2}$ are, respectively, compared with the numerical result of $\pi^{-1}\ln\big(|\beta_{\mathbf{k}\pm}|^2\big)$ and $|\beta_{\mathbf{k}\pm}|^2$ in Figures 5 (for $k_z>0$) and 6 (for $k_z<0$). These figures indicate that $\zeta_0^2$ is negative for the case of complex turning points and therefore, in this case, the pair production is exponentially suppressed. These plots confirm that (as is physically expected) the more larger the pair's mass and momentum are the harder it to be created. Comparing Figures 5 and 6, also, show that the modes with anti-screening orientations ($k_z>0$) are more suppressed than those with screening ($k_z<0$) orientations.

**Case (c)** $\mathcal{M}^2 = \frac{9}{4} - (\sqrt{\alpha} \mp 1)|\beta_\pm|$ **or** $\mathcal{M}^2 = \frac{9}{4} + (\sqrt{\alpha} \pm 1)|\beta_\pm|$**:** In this case, with a real or purely imaginary double turning point $\mathfrak{z}_{1\pm} = \mathfrak{z}_{2\pm}$, we find $\zeta_0^2 = 0$. This can be trivially seen either from the definition (20) or from the expression (30) in which $\mathfrak{m} = 0$ and $K(0) = E(0) = \frac{\pi}{2}$, or the expression (31) in which $\mathfrak{n} = 1$, $\psi = \pi/2$, $F(\pi/2, \mathfrak{n}) = K(\mathfrak{n})$ and $E(\pi/2, \mathfrak{n}) = E(\mathfrak{n})$.

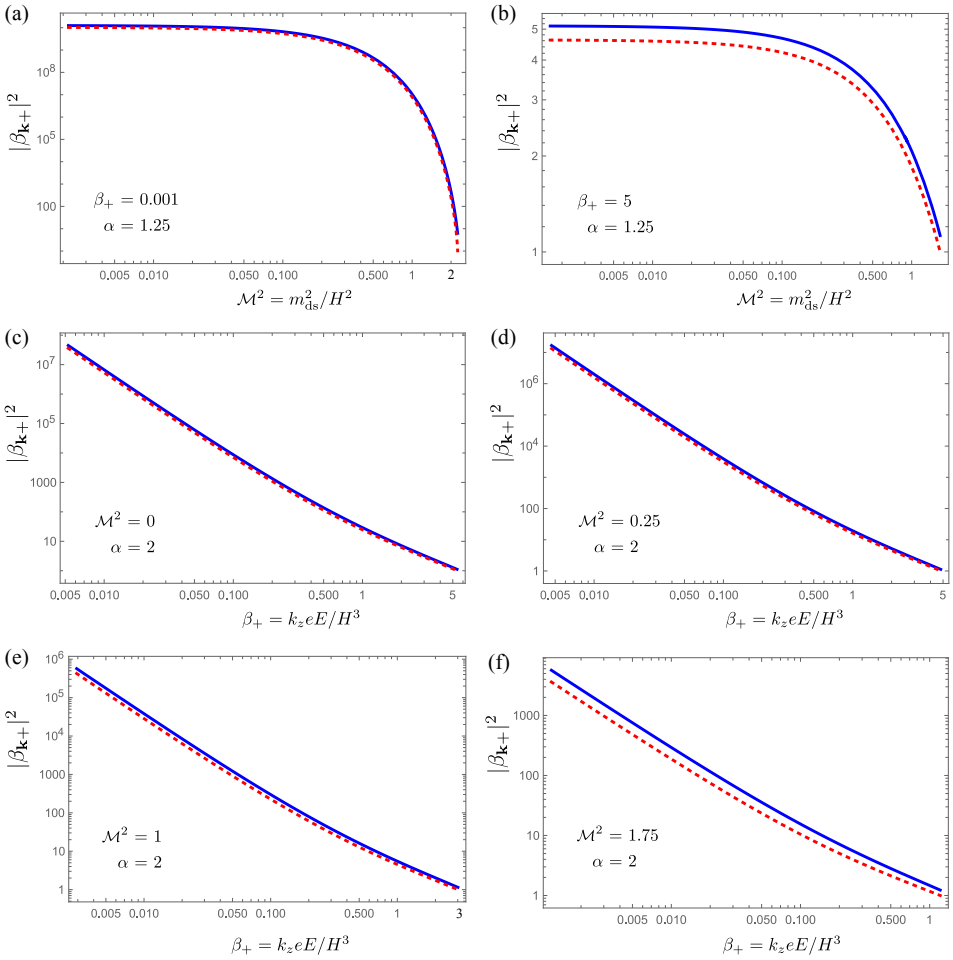


Figure 3: Plots of numerical (exact) (blue solid curves) and approximate analytical (red dotted curves) results of the pair production probability $|\beta_{\mathbf{k}+}|^2$ for $k_z > 0$, with two real turning points. The panels (a) and (b) are plotted for some fixed values of electric field and particle's momentum. At the other figures the particle's mass and momentum are fixed. These figures show that pairs with small masses and momentums are easy to be created.

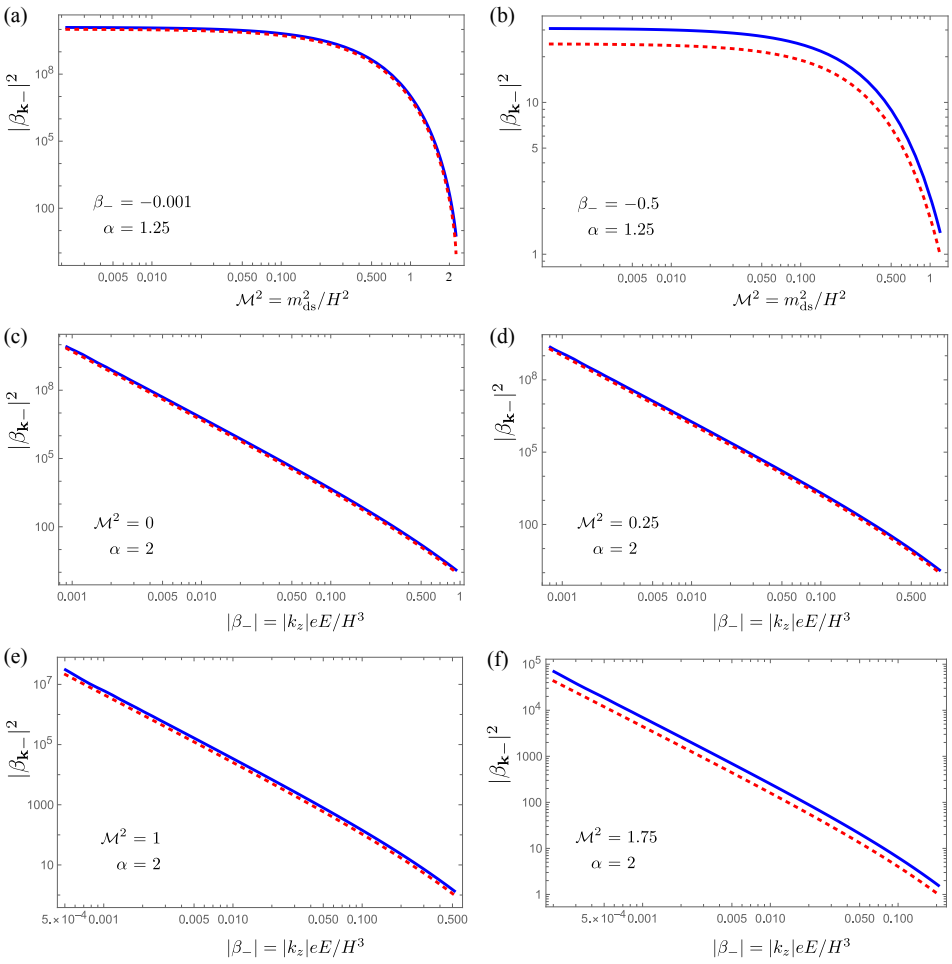


Figure 4: Plots of numerical (exact) (blue solid curves) and approximate analytical (red dotted curves) results of the pair production probability $|\beta_{\mathbf{k}-}|^2$ for $k_z < 0$, with two real turning points. The panels (a) and (b) are plotted for some fixed values of electric field and particle's momentum. At the other figures the particle's mass and momentum are fixed. These figures show that pairs with small masses and momentums are easy to be created.

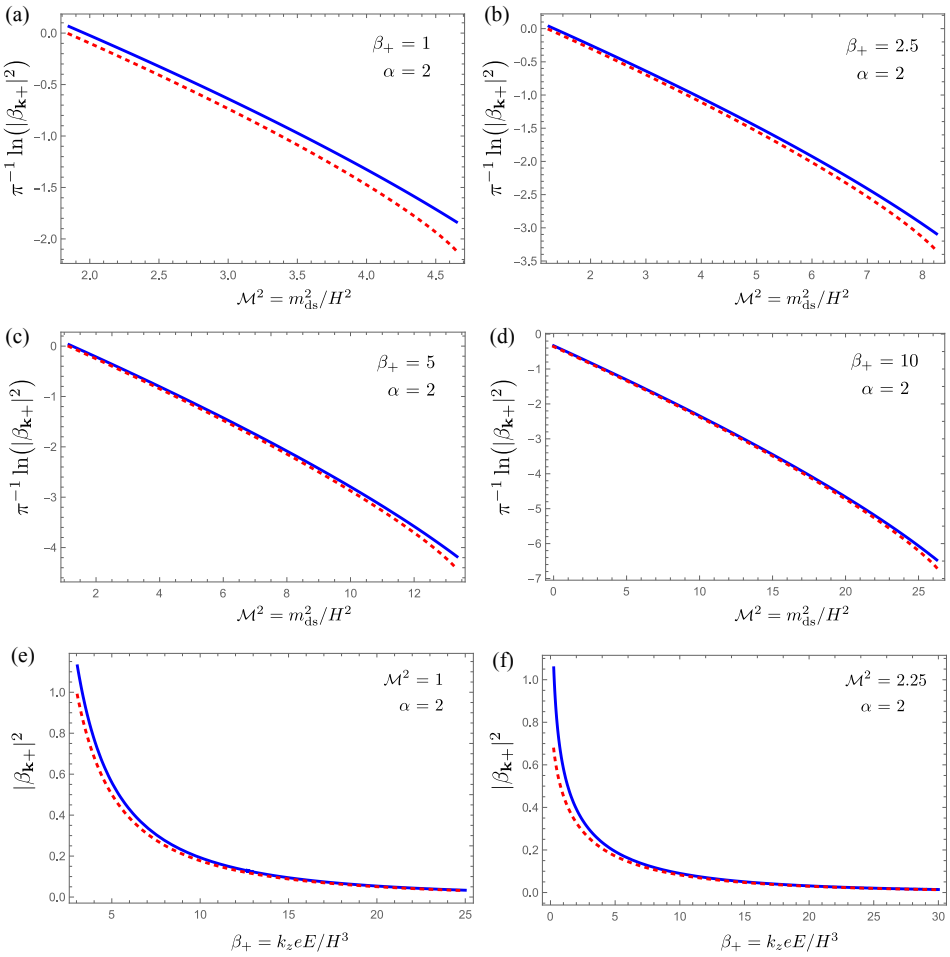


Figure 5: Plots of numerical (exact) (blue solid curves) and approximate analytical (red dotted curves) results of $\lambda\zeta_0^2$ the pair production probability $|\beta_{\mathbf{k}+}|^2$ for $k_z > 0$, with two complex conjugate turning points. $\lambda\zeta_0^2$ is compared with the numerical value of $\pi^{-1}\ln\big(|\beta_{\mathbf{k}+}|^2\big)$ in the panels (a) – (d) for fixed values of the electric field and particle's momentum. At the figures (e) and (f), for some fixed values of the particle's mass and momentum, the approximate result of $|\beta_{\mathbf{k}+}|^2$ is compared with the numerical one. These figures confirm that the Schwinger pairs with large mass or large momentum $k_z$ are hard to be created.

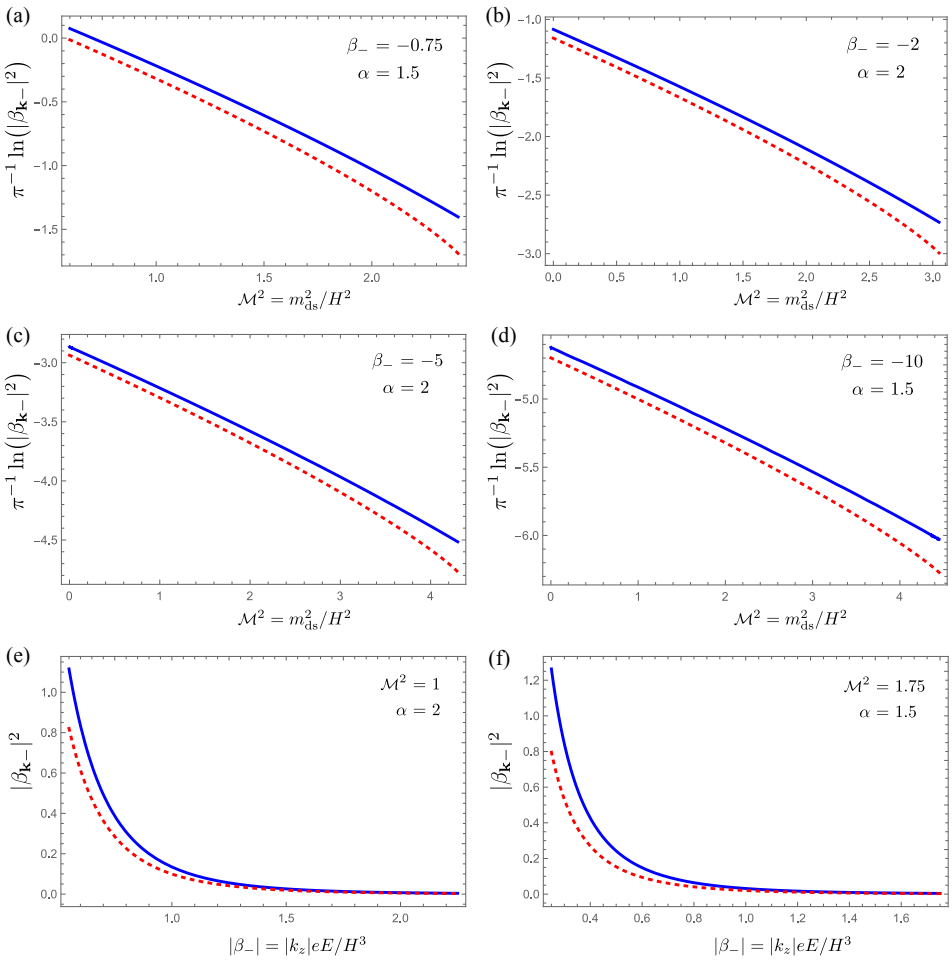


Figure 6: Plots of numerical (exact) (blue solid curves) and approximate analytical (red dotted curves) results of $\lambda\zeta_0^2$ and the pair production probability $|\beta_{\mathbf{k}-}|^2$ for $k_z < 0$, with two complex conjugate turning points. $\lambda\zeta_0^2$ is compared with the numerical value of $\pi^{-1}\ln\big(|\beta_{\mathbf{k}-}|^2\big)$ in the panels (a) – (d) for some fixed values of the particle's mass and momentum. At the figures (e) and (f), for some fixed values of the particle's mass and momentum, the approximate result of $|\beta_{\mathbf{k}-}|^2$ is compared with the numerical one. These figures confirm that the Schwinger pairs with large mass or large momentum $k_z$ are hard to be created.

The numerical value for $|\beta_{\mathbf{k}\pm}|^2$ can be obtained from the numerical solutions of Equation (9). For this purpose, we first notice that when $\mathfrak{z}$ approaches zero, one can choose the positive- and negative-frequency out-modes as (compare with the WKB solution (26))

$$\phi^{(\mathrm{out},+)}_{\mathbf{k}\pm}(\mathfrak{z}) = \frac{\mathfrak{z}}{\sqrt{|k_z|\,|\beta_\pm|}}\,\exp\Big[-i\frac{|\beta_\pm|}{2\mathfrak{z}}\Big], \qquad \phi^{(\mathrm{out},-)}_{\mathbf{k}\pm}(\mathfrak{z}) = \phi^{(\mathrm{out},+)}_{\mathbf{k}\pm}(\mathfrak{z})^*,$$

which solve the asymptotic equation $\mathrm{d}^2\phi_{\mathbf{k}\pm}/\mathrm{d}\mathfrak{z}^2 + \big(\beta^2/(4\mathfrak{z}^2)\big)\phi_{\mathbf{k}\pm} = 0$ and are normalized with the inner product $\big(\phi_1(\mathfrak{z}),\phi_2(\mathfrak{z})\big) = i\big[\phi_1(\mathfrak{z})^*\,\phi_2'(\mathfrak{z}) - \phi_1'(\mathfrak{z})^*\,\phi_2(\mathfrak{z})\big]$, where $\phi' = \partial_\tau\phi = -|k_z|\partial_\mathfrak{z}\phi$. Also, we take the expression (21) as the initial condition to obtain the numerical solution $\phi_{\mathbf{k}\pm}(\mathfrak{z})$ and its derivative. Then, according to the expansion $\phi_{\mathbf{k}\pm}(\mathfrak{z}) = \alpha_{\mathbf{k}\pm}\,\phi^{(\mathrm{out},+)}_{\mathbf{k}\pm}(\mathfrak{z}) + \beta_{\mathbf{k}\pm}\,\phi^{(\mathrm{out},-)}_{\mathbf{k}\pm}(\mathfrak{z})$, we can use a very small value for $\mathfrak{z}$ ($\mathfrak{z}\to 0$) to compute $|\beta_{\mathbf{k}\pm}|^2 = \big|\big(\phi_{\mathbf{k}\pm}(\mathfrak{z}),\phi^{(\mathrm{out},-)}_{\mathbf{k}\pm}(\mathfrak{z})\big)\big|^2$. This numerical result is compared with the analytical value $|\beta_{\mathbf{k}\pm}|^2 = e^{\pi\lambda\zeta_0^2}$ in Figures 3 and 5 for $k_z > 0$ and Figures 4 and 6 for $k_z < 0$.

### 3.3 Weak Electric Field Limit

For the weak electric field $eE \ll H^2$ ($\mathcal{E} \ll 1$), the parameter $|\beta_\pm|$ is small, and hence the modulus $\mathfrak{m}$ of the elliptic functions is close to one. This means that the *complementary modulus* $\mathfrak{m}' := \sqrt{1-\mathfrak{m}^2}$ is small and one can use the series expansions [13]

$$\begin{aligned} K(\mathfrak{m}) &= \ln\frac{4}{\mathfrak{m}'} + \frac{1}{4}\Big(\ln\frac{4}{\mathfrak{m}'} - 1\Big)\mathfrak{m}'^2 + \frac{9}{64}\Big(\ln\frac{4}{\mathfrak{m}'} - \frac{7}{6}\Big)\mathfrak{m}'^4 + \cdots,\\ E(\mathfrak{m}) &= 1 + \frac{1}{2}\Big(\ln\frac{4}{\mathfrak{m}'} - \frac{1}{2}\Big)\mathfrak{m}'^2 + \frac{3}{16}\Big(\ln\frac{4}{\mathfrak{m}'} - \frac{13}{12}\Big)\mathfrak{m}'^4 + \cdots, \end{aligned}$$

for the elliptic functions in Equation (30) to find the approximate value of $\zeta_0^2$ in the powers of $\beta_\pm$ (or $E$). The result is

$$\begin{aligned} \pi\lambda\zeta_0^2 &\simeq 2\sqrt{\mu^2}\Big\{-2 + \Big(1 \pm \frac{|\beta_\pm|}{2\mu^2}\Big)\ln\Big(\frac{8\mu^2}{|\beta_\pm|\sqrt{\alpha}}\Big) + \mathcal{O}(\beta_\pm^2)\Big\}\\ &= \sqrt{\frac{9}{4} - \frac{m_{\mathrm{ds}}^2}{H^2}}\,\Bigg\{6\ln 2 - 4 + 2\ln\Big(\frac{9}{4} - \frac{m_{\mathrm{ds}}^2}{H^2}\Big) - \ln\Big(1 + \frac{k_\perp^2}{k_z^2}\Big) - 2\ln\Big(\frac{eE|k_z|}{H^3}\Big)\\ &\qquad \pm\Big(\frac{eE|k_z|}{H^3}\Big)\Big(\frac{9}{4} - \frac{m_{\mathrm{ds}}^2}{H^2}\Big)^{-1}\ln\Big(8\Big(\frac{9}{4} - \frac{m_{\mathrm{ds}}^2}{H^2}\Big)\Big(1 + \frac{k_\perp^2}{k_z^2}\Big)^{-1/2}\Big)\\ &\qquad \mp\Big(\frac{9}{4} - \frac{m_{\mathrm{ds}}^2}{H^2}\Big)^{-1}\Big(\frac{eE|k_z|}{H^3}\Big)\ln\Big(\frac{eE|k_z|}{H^3}\Big) + \mathcal{O}(E^2)\Bigg\}, \end{aligned} \tag{32}$$

where we recall that $k_\perp^2 = k_x^2 + k_y^2$. Thus, in view of the result (32), in the weak electric field limit, pair production probability $|\beta_{\mathbf{k}\pm}|^2 = e^{\pi\lambda\zeta_0^2}$ behaves as

$$|\beta_{\mathbf{k}\pm}|^2 \propto \left(\frac{H^3}{eE|k_z|}\right)^{2\sqrt{\frac{9}{4}-\frac{m_{\rm ds}^2}{H^2}}},$$

which diverges as $eE|k_z|/H^3 \to 0$ (see Figures 3-c to 3-f and 4-c to 4-f).

Though we can not compute the renormalized induced electric current (because we have not at hand any everywhere-defined expression for the mode functions $\phi_{\mathbf{k}\pm}(\mathfrak{z})$), instead, following [8], in the weak electric field limit, we can find the semiclassical current $J$ as

$$J \propto \left(|\beta_{\mathbf{k}-}|^2 - |\beta_{\mathbf{k}+}|^2\right) \approx \mathscr{C}\left(\frac{eE|k_z|}{H^3}\right)^{1-2\sqrt{\frac{9}{4}-\frac{m_{\rm ds}^2}{H^2}}}\left[1-\ln\Big(\frac{eE|k_z|}{H^3}\Big)\right] + \mathcal{O}(E^\delta),$$

where $\delta = 2 - 2\sqrt{9/4 - m_{\rm ds}^2/H^2}$ and

$$\mathscr{C} := -2\left(\mu^2\right)^{-1/2} e^{-4\sqrt{\mu^2}}\Big(\frac{64(\mu^2)^2}{\alpha}\Big)^{\sqrt{\mu^2}}\ \ln\Big(\frac{8\mu^2}{\sqrt{\alpha}}\Big).$$

Similar to the case studied in [11], there exists a critical mass $m_{\rm cr} = \sqrt{2}H$, below which the electric current $J$ exhibits the so-called *infrared hyperconductivity*, which has been initially observed in [8] (only for $m = 0$ in the presence of a uniform electric field background in $(1+1)$-dimensional de Sitter space). Indeed, for $m_{\rm ds} \in (0, \sqrt{2}H)$, when $E$ goes to zero, the electric current $J$ diverges as $1/E^{\,2\Delta}$, where $\Delta := \sqrt{9/4 - m_{\rm ds}^2/H^2} - \frac{1}{2} \in (0, 1)$. In particular, when $m_{\rm ds} = 0$, $J$ is inversely proportional to $E^2$. This divergence behavior is two times faster than the cases considered in [8, 11]. In addition, unlike the case of [11], here for $m_{\rm ds} = m_{\rm cr} = \sqrt{2}H$, $J$ exhibits also a logarithmic divergence in the limit $eE|k_z|/H^3 \to 0$.

# 5. Conclusion

In this work, we have investigated the Schwinger pair creation by a time-dependent electric field in (1+3)-dimensional de Sitter spacetime. Specifically, in $dS_4$, we have considered a charged scalar field, as a test field, coupled to a time-dependent background electric field (3) which has a time-dependent energy density in the expanding universe. We have seen that, while the field equation of motion does not admit an exact analytical solution, it can be solved by means of Olver's uniform asymptotic approximation method. We showed that the equation of motion, in general, has two turning points, whose natures (single, double, real or complex) depend on the value of the electric field $E$, the particle's mass $m$, and wave vector $\mathbf{k}$. Using the first-order approximate solutions (the mode functions for the canonical

quantization) the Bogoliubov coefficients and consequently the probability for the pair production were computed both analytically and numerically, which strictly depends on the natures of the turning points. More precisely, we found that the pair creation process is enhanced when the two turning points are real and single, and suppressed when they are complex conjugate. Furthermore, when the particle's mass and momentum are small, two turning points are real, and the more smaller are the easier to create particles by the Schwinger mechanism. For massive particles or large momentums, both turning points are complex, and the Schwinger pair creation is exponentially suppressed. In addition, for both cases of real and complex turning points, we explored that the modes with anti-screening orientation ($k_z > 0$) are different from those with screening orientation ($k_z < 0$) in pair production process. Indeed, light (massive) particles with anti-screening orientations are hardest to be produced (are more suppressed) than those with screening orientations.

For small particle's mass and momentum, in the weak electric field limit, we also computed analytically the pair production probability and the semi-classical electric current induced by the created Schwinger pairs. Remarkably, we found that the pair creation probability $|\beta_{\mathbf{k}\pm}|^2$ and hence the semi-classical current $J$ are strongly enhanced as the electric field diminishes. Indeed, as $E \to 0$, pair creation probability and the semi-classical current diverge, respectively, as $1/E^{2\Delta+1}$ and $1/E^{2\Delta}\,(1-\ln E)$, where $\Delta := \sqrt{9/4 - m_{\rm ds}^2/H^2} - \frac{1}{2} \in (0,1)$. This means that, similar to the case studied in [11], there exists a critical mass $m_{\rm cr} = \sqrt{2}H$, below which the electric current J exhibits the so-called infrared hyperconductivity that stems from the infrared behavior of light fields in de Sitter spacetime. For a constant electric field background, this negative conductivity shows itself in the regularized electric current [3, 8, 21]. But, it is recently argued in [1] that this spurious is a byproduct of nonlinear corrections to the Maxwell action and the logarithmic running of the coupling constant.

## Appendix: Weber's Equation, Parabolic Cylinder Functions and their Asymptotic Expansion

In this appendix, we present the detailed derivation of the general solution (19) of equation $\mathrm{d}^2U/\mathrm{d}\zeta^2 = \left[\lambda^2(\zeta_0^2 - \zeta^2)\right] U$, and elaborate on their asymptotic expansions. It can be easily seen that in terms of the variable $\tilde{\zeta} := \sqrt{\lambda}\,(1-i)\zeta = \sqrt{2\lambda}\,\zeta\, e^{-i\pi/4}$, this equation can be cast into the form of the so-called Weber's equation [40]

$$\frac{\mathrm{d}^2U}{\mathrm{d}\tilde{\zeta}^2} + \left[\frac{1}{2} + \nu - \frac{1}{4}\,\tilde{\zeta}^2\right] U = 0, \tag{33}$$

where $\nu := -\frac{1}{2} - \frac{i}{2}\,\lambda\,\zeta_0^2$. The parabolic cylinder functions $D_\nu(\tilde{\zeta})$ satisfy the differential equation (33). Because Equation (33) is unaltered if we simultaneously apply the changes $\tilde{\zeta} \to i\tilde{\zeta}$ and $\nu \to -\nu - 1$, we can choose $D_\nu(\sqrt{2\lambda}\,\zeta\, e^{-i\pi/4})$ and $D_{-\nu-1}(\sqrt{2\lambda}\,\zeta\, e^{i\pi/4})$ as two linearly independent solutions of equation $\mathrm{d}^2U/\mathrm{d}\zeta^2 =$

$\left[\lambda^2(\zeta_0^2-\zeta^2)\right]U$. Thus, the general asymptotic solution near two turning points $\mathfrak{z}_1$ and $\mathfrak{z}_2$ can be written as in Equation (19).

Next, in view of the relation $D_\nu(\tilde{\zeta})=U(-\frac{1}{2}-\nu,\tilde{\zeta})$ and the asymptotic expansions for Weber parabolic cylinder function $U(a,\tilde{\zeta})$ that is given in [25], we observe that the asymptotic expansion of $D_\nu(\tilde{\zeta})$ of large order $\zeta_0^2$ in the limit $\zeta\to+\infty$ can be expressed as

$$D_{-\frac{1}{2}-\frac{i}{2}\lambda\zeta_0^2}(\sqrt{2\lambda}\,\zeta\,e^{-i\pi/4}) \;\simeq\; \frac{e^{i\lambda\,\zeta_0^2\,\xi(\zeta)}}{(\zeta^2-\zeta_0^2)^{1/4}}\,h(\sqrt{\lambda}\zeta_0\,e^{-i\pi/4}), \tag{34}$$

$$D_{-\frac{1}{2}+\frac{i}{2}\lambda\zeta_0^2}(\sqrt{2\lambda}\,\zeta\,e^{i\pi/4}) \;\simeq\; \frac{e^{-i\lambda\,\zeta_0^2\,\xi(\zeta)}}{(\zeta^2-\zeta_0^2)^{1/4}}\,h(\sqrt{\lambda}\zeta_0\,e^{i\pi/4}), \tag{35}$$

where $\xi(\zeta)$ is defined by

$$\zeta_0^2\,\xi(\zeta):=\int_{\zeta_0}^{\zeta}\mathrm{d}\zeta'\sqrt{\zeta'^2-\zeta_0^2}=\frac{1}{2}\zeta\sqrt{\zeta^2-\zeta_0^2}-\frac{1}{2}\zeta_0^2\,\mathrm{arccosh}(\zeta/\zeta_0),$$

$h(\sqrt{\lambda}\zeta_0\,e^{-i\frac{\pi}{4}})$ is approximately given by

$$h(\sqrt{\lambda}\zeta_0\,e^{-i\pi/4})\simeq(2\lambda)^{-\frac{1}{4}}\,e^{-\pi\frac{\lambda\zeta_0^2}{8}}\,e^{i(\frac{\pi}{8}-\frac{1}{2}\phi_2)},$$

$h(\sqrt{\lambda}\zeta_0e^{i\frac{\pi}{4}})=(h(\sqrt{\lambda}\zeta_0e^{-i\frac{\pi}{4}}))^*$, and $\phi_2:=\mathrm{ph}\Gamma\left(\frac{1}{2}+\frac{i}{2}\lambda\zeta_0^2\right)$ is the phase of $\Gamma\left(\frac{1}{2}+\frac{i}{2}\lambda\zeta_0^2\right)$.

To find the asymptotic expansion of $D_\nu(\sqrt{2\lambda}\,\zeta\,e^{-i\pi/4})$ of large order $\zeta_0^2$ in the limit $\zeta\to-\infty$, we use the connection formula [40, 28]

$$D_\nu(-\sqrt{2\lambda}\zeta e^{-i\frac{\pi}{4}})=e^{i\pi\nu}D_\nu(\sqrt{2\lambda}\zeta e^{-i\frac{\pi}{4}})+i\,e^{i\pi\nu/2}\frac{\sqrt{2\pi}}{\Gamma(-\nu)}\,D_{-\nu-1}(\sqrt{2\lambda}\zeta e^{i\frac{\pi}{4}}). \tag{36}$$

Substituting Equations (34) and (35) in Equation (36) and making use of the identities $ie^{-i\pi/4}h(\sqrt{\lambda}\zeta_0e^{i\frac{\pi}{4}})=h(\sqrt{\lambda}\zeta_0e^{-i\frac{\pi}{4}})$ and

$$\Gamma(\frac{1}{2}+\frac{i}{2}\lambda\zeta_0^2)=\sqrt{\pi}(\cosh(\frac{\pi\lambda\zeta_0^2}{2}))^{-1/2}\,e^{i\phi_2},$$

we find that, for large order $\zeta_0^2$, the asymptotic form of $D_\nu(\sqrt{2\lambda}\,\zeta\,e^{-i\pi/4})$ in the limit $\zeta\to-\infty$ can be written as

$$D_{-\frac{1}{2}-\frac{i}{2}\lambda\zeta_0^2}(\sqrt{2\lambda}\,\zeta\,e^{-i\pi/4}) \;\simeq\; \frac{h(\sqrt{\lambda}\zeta_0\,e^{-i\pi/4})}{(\zeta^2-\zeta_0^2)^{1/4}}\Big[\sqrt{1+e^{\pi\lambda\zeta_0^2}}\,e^{-i\lambda\,\zeta_0^2\,\xi'(\zeta)} -ie^{\pi\lambda\zeta_0^2/2}\,e^{i\lambda\,\zeta_0^2\,\xi'(\zeta)}\Big], \tag{37}$$

where $\xi'(\zeta)$ is defined by

$$\zeta_0^2\,\xi'(\zeta):=\int_{-\zeta_0}^{\zeta}\mathrm{d}\zeta'\sqrt{\zeta'^2-\zeta_0^2}=-\frac{1}{2}\zeta\sqrt{\zeta^2-\zeta_0^2}-\frac{1}{2}\zeta_0^2\,\mathrm{arccosh}(-\zeta/\zeta_0).$$

**Conflicts of Interest.** The authors declare that there are no conflicts of interest regarding the publication of this article.

## References

[1] M. Banyeres, G. Domènech and J. Garriga, Vacuum birefringence and the Schwinger effect in (3+1) de Sitter, *J. Cosmol. Astropart. Phys.* **10** (2018) 023.

[2] D. Baumann and L. McAllister, *Inflation and String Theory*, Cambridge University Press, Cambridge, UK, 2015.

[3] E. Bavarsad, C. Stahl and S. -S. Xue, Scalar current of created pairs by Schwinger mechanism in de Sitter spacetime, *Phys. Rev. D* **94** (2016) 104011.

[4] R. G. Cai and S. P. Kim, One-loop effective action and Schwinger effect in (anti-) de Sitter space, *J. High Energy Phys.* **09** (2014) 072.

[5] S. M. Carroll, The Cosmological Constant, *Living Rev. Relativity* **3** (2001) $1-56$.

[6] A. Di Piazza, C. Müller, K. Z. Hatsagortsyan and C. H. Keitel, Extremely high-intensity laser interactions with fundamental quantum systems, *Rev. Mod. Phys.* **84** (2012) $1117-1228$.

[7] R. Emami, H. Firouzjahi, S. M. Sadegh Movahed and M. Zarei, Anisotropic inflation from charged scalar fields, *J. Cosmol. Astropart. Phys.* **02** (2011) 005.

[8] M. B. Fröb, J. Garriga, S. Kanno, M. Sasaki, J. Soda, T. Tanaka and A. Vilenkin, Schwinger effect in de Sitter space, *J. Cosmol. Astropart. Phys.* **04** (2014) 009.

[9] J. Garriga, Pair production by an electric field in (1+1)-dimensional de Sitter space, *Phys. Rev. D* **49** (1994) $6343-6346$.

[10] F. Gelis and N. Tanji, Schwinger mechanism revisited, *Prog. Part. Nucl. Phys.* **87** (2016) $1-49$.

[11] J.-J. Geng, B.-F. Li, J. Soda, A. Wang, Q. Wu and T. Zhu, Schwinger pair production by electric field coupled to inflaton, *J. Cosmol. Astropart. Phys.* **02** (2018) 018.

[12] M. Giovannini, Spectator electric fields, de Sitter spacetime, and the Schwinger effect, *Phys. Rev. D* **97** (2018) 061301(R).

[13] I. S. Gradshteyn and I. M. Ryzhik, *Table of Integrals, Series and Products*, 7th ed., Academic Press, Amsterdam, 2007.

[14] S. Haouat and R. Chekireb, Effect of electromagnetic fields on the creation of scalar particles in a flat Robertson-Walker spacetime, *Eur. Phys. J. C* **72** (2012) 2034.

[15] S. Haouat and R. Chekireb, Schwinger effect in a Robertson-Walker spacetime, *Int. J. Theor. Phys.* **51** (2012) 1704 – 1714.

[16] T. Hayashinaka, T. Fujita and J. Yokoyama, Fermionic Schwinger effect and induced current in de Sitter space, *J. Cosmol. Astropart. Phys.* **07** (2016) 010.

[17] T. Hayashinaka and J. Yokoyama, Point splitting renormalization of Schwinger induced current in de Sitter spacetime, *J. Cosmol. Astropart. Phys.* **07** (2016) 012.

[18] W. Heisenberg and H. Euler, Consequences of Dirac's theory of positrons, *Z. Phys.* **98** (1936) 714 – 732.

[19] S. P. Kim and D. N. Page, Schwinger pair production in $dS_2$ and $AdS_2$, *Phys. Rev. D* **78** (2008) 103517.

[20] H. Kitamoto, Schwinger effect in inflation-driven electric field, *Phys. Rev. D* **98** (2018) 103512.

[21] T. Kobayeshi and N. Afshordi, Schwinger effect in 4D de Sitter space and constraints on magnetogenesis in the early Universe, *J. High Energy Phys.* **10** (2014) 166.

[22] J. Martin, *Inflationary Perturbations: The Cosmological Schwinger Effect*, in: Inflationary Cosmology, Lecture Notes in Physics, vol. 738, 193 – 241, Springer-Verlag, Berlin, 2007.

[23] S. Moradi, Particle production in cosmological spacetimes with electromagnetic fields, *Mod. Phys. Lett. A* **24** (2009) 1129 – 1136.

[24] A. H. Nayfeh, *Perturbation Methods*, Wiley, New York, 1973.

[25] F. W. J. Olver, Uniform asymptotic expansions for Weber parabolic cylinder functions of large orders, *J. Res. Nat. Bur. Standards, Sect. B: Math. and Math. Phys.* **63B** (1959) 131 – 169.

[26] F. W. J. Olver, Second-order linear differential equations with two turning points, *Philos. Trans. Roy. Soc. A* **278** (1975) 137 – 174.

[27] F. W. J. Olver, *Asymptotics and Special Functions*, AKP Classics, Wellesley, MA, 1997.

[28] F. W. J. Olver, D. W. Lozier, R. F. Boisvert and C. W. Clark, *NIST Handbook of Mathematical Functions*, Cambridge University Press, Cambridge, UK, 2010.

[29] L. Parker and D. Toms, *Quantum Field Theory in Curved Space: Quantized Fields and Gravity*, Cambridge University Press, Cambridge, UK, 2009.

[30] R. Ruffini, G. Vereshchagin and S. S. Xue, Electron-positron pairs in physics and astrophysics: from heavy nuclei to black holes, *Phys. Rept.* **487** (2010) 1 – 140.

[31] F. Sauter, Über das verhalten eines electrons im homogenen electrischen feld nach der relativistischen theorie Diracs, *Z. Phys.* **69** (1931) 742 – 764.

[32] J. S. Schwinger, On gauge invariance and vacuum polarization, *Phys. Rev.* **82** (1951) 664 – 679.

[33] S. Shakeri, M. A. Gorji and H. Firouzjahi, Schwinger mechanism during inflation, *Phys. Rev. D* **99** (2019) 103525.

[34] R. Sharma and S. Singh, Multifaceted Schwinger effect in de Sitter space, *Phys. Rev. D* **96** (2017) 025010.

[35] K. Sogut, A. Havare, On the scalar particle creation by electromagnetic fields in Robertson-Walker spacetime, *Nucl. Phys. B* **901** (2015) 76 – 84.

[36] C. Stahl, E. Strobel and S.-S. Xue, Fermionic current and Schwinger effect in de Sitter spacetime, *Phys. Rev. D* **93** (2016) 025004.

[37] V. M. Villalba, Creation of spin-$\frac{1}{2}$ particles by an electric field in de Sitter space, *Phys. Rev. D* **52** (1995) 3742 – 3745.

[38] V. M. Villalba and W. Greiner, Creation of scalar and Dirac particles in the presence of a time varying electric field in an anisotropic Bianchi type I universe, *Phys. Rev. D* **65** (2001) 025007.

[39] M.-a. Watanabe, S. Kanno and J. Soda, Inflationary universe with anisotropic hair, *Phys. Rev. Lett.* **102** (2009) 191302.

[40] E. T. Whittaker and G. N. Watson, *A Course of Modern Analysis*, 2nd ed., Cambridge University Press, Cambridge, UK, 1915.

[41] T. Zhu, A. Wang, G. Cleaver, K. Kirsten and Q. Sheng, Constructing analytical solutions of linear perturbations of inflation with modified dispersion relations, *Int. J. Modern Phys. A* **29** (2014) 1450142.

[42] T. Zhu, A. Wang, G. Cleaver, K. Kirsten and Q. Sheng, Inflationary cosmology with nonlinear dispersion relations, *Phys. Rev. D* **89** (2014) 043507.

[43] T. Zhu, A. Wang, G. Cleaver, K. Kirsten and Q. Sheng, Gravitational quantum effects on power spectra and spectral indices with higher-order corrections, *Phys. Rev. D* **90** (2014) 063503.

[44] T. Zhu, A. Wang, K. Kirsten, G. Cleaver and Q. Sheng, High-order primordial perturbations with quantum gravitational effects, *Phys. Rev. D* **93** (2016) 123525.

Fatemeh Monemi
Department of Physics,
University of Kashan,
Kashan, I. R. Iran
e-mail: f-monemi@grad.kashanu.ac.ir

Farhad Zamani
Department of Physics,
University of Kashan,
Kashan, I. R. Iran
e-mail: zamani@kashanu.ac.ir